Selenium Nanoparticles: A Small-Angle Neutron Scattering Study

J. A. Johnson, Marie-Louise Saboungi,* P. Thiyagarajan, R. Csencsits, and D. Meisel†

Argonne National Laboratory, Argonne, Illinois 60439

Received: July 30, 1998; In Final Form: October 19, 1998

The growth process of selenium nanoparticles prepared in a microemulsion by a reverse micelle method is probed by several techniques. The smallest particles synthesized are of the order of 40 Å in diameter, producing the usual blue shift in the optical spectra. An amorphous to crystalline phase transition was detected by both electron and X-ray diffraction. The micelle structure investigated by small-angle neutron scattering was found to be unaffected by the conditions of the reaction.

1. Introduction

Particles synthesized on a nanometer scale by the reverse micelle method are of interest for the changes in electrical and optical properties brought about by the size reduction. Microemulsions produced by this method consist of a water core surrounded by a surfactant dispersed in an oil medium. The core size is controlled by the water to surfactant concentration ratio, which in turn controls the resulting particle size.[1]

Selenium is used in rectifiers, solar cells, photographic exposure meters, and xerography. It is also used in the glass industry to eliminate bubbles and remove undesirable tints produced by iron. It exists in a number of crystalline structures, the principal ones being trigonal, consisting of helical chains, and the less stable monoclinic, consisting of Se_8 rings.[2] Monoclinic Se (m-Se) comes in three forms: α, β, and γ, which differ only in the way the rings are packed.[3,4] Amorphous selenium (a-Se) is composed of a mixture of disordered chains.

Previous attempts to synthesize nanometer-scale particles of selenium have used γ-radiation of solutions[5] and crystallization of melt-quenched amorphous selenium.[6] Both of these methods produced trigonal selenium, but the size distribution was slightly different, with the first method yielding 80−170 Å and the second 60−450 Å particles.

Amorphous selenium with a mean particle size of 20 Å has been synthesized in aqueous solution by Dimitrijevic et al.[9] The solutions, however, are subject to extreme photocorrosion and are stable for only a few hours.

Selenium has been incorporated into various forms of zeolite and identified by optical and Raman spectroscopy and anomalous X-ray scattering.[7,8] The diameter of the zeolite supercages is about 13 Å, which restricts the size of the selenium entities. Chains and/or rings of selenium are produced, depending on the nature of the countercation and the zeolite used.

In this study, nanoparticles of selenium were synthesized in a reverse-micelle medium on an intermediate length scale of 20−200 Å and characterized by transmission electron microscopy (TEM), optical spectroscopy, and X-ray diffraction. The micelle structure was examined with small-angle neutron scattering (SANS).

2. Experimental Procedures

Sodium bis(2-ethylhexyl)sulfosuccinate usually called AOT (obtained from Aldrich and used without further purification) was dissolved in heptane to make a 0.1 M solution. Three values of w (=[H_2O]/[AOT]) were used, namely 5, 10, and 20. The appropriate amount of Nanopure water required to give the desired w was added to the heptane−AOT solution, and the mixture was stirred for several hours to ensure equilibrium. The solution of heptane, AOT, and water was fully deoxygenated by bubbling ultrahigh-purity argon through the mixture. Selenious acid (H_2SeO_3) was added to half of the solution to give a concentration of 2.0×10^{-3} M, and the same molar amount of hydrazine was added to the other half; both chemicals were predissolved in deoxygenated Nanopure water. After several hours, these two solutions were combined, initiating the reaction

$$H_2SeO_3 + N_2H_42(HCl) \rightarrow Se\downarrow + N_2\uparrow + 3H_2O + 2HCl \quad (1)$$

inside the water pool. These operations were carried out inside a nitrogen-filled glovebox.

In all the experiments, an orange-red precipitate was obtained that was identified as selenium by energy-dispersive X-ray spectrometry (EDS). The color implied that its form was either amorphous or monoclinic since trigonal selenium is black. It should be noted that nanoparticles could not be isolated by traditional capping techniques[1] but no changes in color or X-ray patterns were noticed in samples aged up to 2 weeks. The solution went from colorless to pale yellow to orange during the first 15 min of reaction time, and samples were removed from solution at several times (1, 2, 5, 10, 15, and 30 min) after the reaction initiation and placed on carbon grids for examination by electron microscopy. The rate of color change varied with the concentration of selenious acid and hydrazine and the value of w. After about 2 h, a red-orange precipitate was deposited at the bottom of the flask. The solution was then centrifuged to extract the particles, which were washed in heptane and methanol to remove any residual AOT and water. Drying with petroleum ether and under vacuum changed the color of the particles from red to black so instead, the methanol was allowed to evaporate slowly. However, in samples prepared at high pH (by adding 5 mL of 10 M NaOH immediately after the solutions containing selenious acid and hydrazine had been mixed), the color change was much slower to appear.

Transmission electron microscopy (TEM) was performed on a JEOL 100CXII equipped with an EDS that confirmed the

* Corresponding author.
† Present address: Radiation Laboratory, University of Notre Dame, Notre Dame, Indiana.

10.1021/jp983229y CCC: $18.00
Published on Web 12/11/1998

presence of selenium in the particles. Absorbance spectra were measured on a Varian Cary 5G UV−vis−NIR spectrophotometer over a wavelength range, 200−800 nm, at time intervals of 15 min. A sample of approximately 3 mL was extracted from the mixture immediately after the reaction had started and placed in a quartz cuvette to observe the changes in the optical properties over a period of 2 h. A mixture of heptane, AOT, and water was used as a reference, and the background was subtracted automatically.

The precipitation rate of the selenium increases with concentration, so the concentration was tailored to the particular technique employed. For optical spectroscopy, a threshold concentration of 2.0×10^{-3} M was required to record the spectra. At a concentration of 5.0×10^{-4} M or below, the particles remained in suspension indefinitely, enabling the collection of neutron scattering data over a period of 2 h. TEM and X-ray techniques were not sensitive to the quantity of sample obtained in the present range of concentration.

The scattering measurements were carried out with the small-angle neutron diffractometer[10] at the Intense Pulsed Neutron Source, Argonne National Laboratory. The wavelength range of the neutrons was 0.5−14.0 Å, measured by time-of-flight with a resolution $\Delta t/t = 0.05$. The instrument can provide useful SANS data in the momentum transfer (q) range of 0.0035−0.8 $Å^{-1}$ in a single measurement ($q = (4\pi/\lambda) \sin \theta$, where θ is half the scattering angle and λ is the wavelength of the incident neutrons). The scattering data were corrected following a standard procedure[11] for empty cell, instrument background scattering, detector sensitivity, and sample transmission and were presented on an absolute scale.

In all samples used for SANS ($w = 10$), heptane was replaced by fully deuterated cyclohexane-d_{12} to increase the contrast for the scattering from AOT while reducing the contrast for water (or D_2O). That is the only way one can see the core−shell structure of the reverse micelles. Three samples were prepared in C_6D_{12} containing AOT alone, AOT with D_2O, and AOT with D_2O and Se; they were contained in quartz cells with a path length of 2 mm. The cells were sealed in order to protect the samples from air. All experiments were performed at room temperature.

Eastoe et al[12] have examined the water core radius in the presence of several solvents and found it to be insensitive to the chain length and density of the oil in all *n*-alkanes C_4-C_{12} and in cyclohexane. We therefore expect no significant differences between the radii of the reverse micelles in cyclohexane compared to heptane.

3. Results and Discussion

TEM showed nanoparticles of selenium with a spherical shape and a size ranging from 40 to 3000 Å. As an example, Figure 1 shows Se particles of 40−250 Å with a median size of 100 Å. Electron diffraction showed the selenium to be a mixture of amorphous and monoclinic particles; even though the diffraction spots from the small particles are diffuse, they are peaked at specific Bragg locations, while amorphous materials diffract according to a Patterson distribution.[13] When NaOH was added to the micelle solution, TEM showed that particles removed from solution after 15 min were 50 Å in diameter. Without the addition of NaOH, samples examined at corresponding times were of the order of 200 Å in diameter.

Representative absorbance spectra are shown at the reaction times specified for $w = 5$ in Figure 2; they all exhibit a shoulder around 2.3 eV that increased in intensity and shifted during a reaction time of approximately 2 h, after which the absorbance

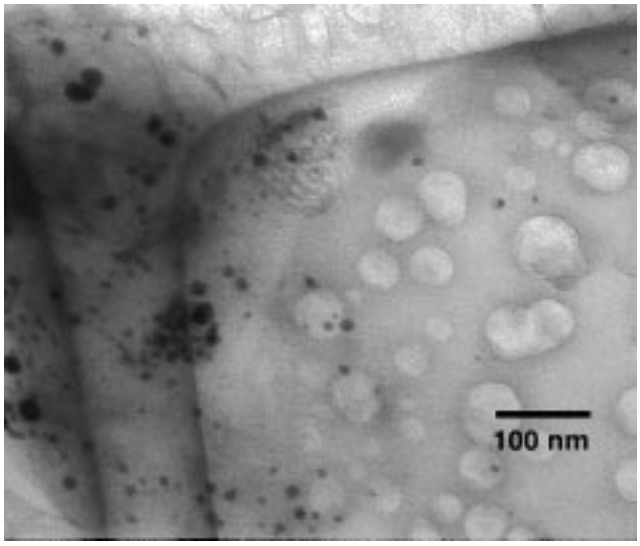

Figure 1. TEM of selenium particles.

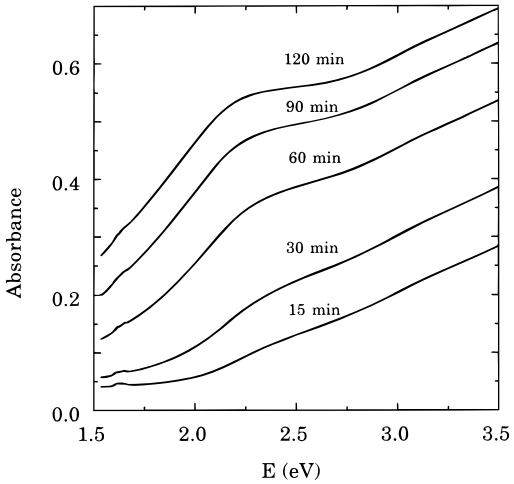

Figure 2. Absorbance spectra for selenium particles at $w = 5$.

level remained constant. Before an observation time of 15 min, no discernible spectral shape was visible. It is assumed that the reaction is complete after a few minutes and changes observed are due only to the increased size of the particles. It is possible that Ostwald ripening[14] may occur during this process and lead to a wide distribution in particle size.

X-ray diffraction spectra showed that the sample was α-monoclinic, which has a direct allowed optical transition.[15] This transition is characterized by a linear variation of $(\alpha h\nu)^2$ with $h\nu$, where α is the absorption coefficient and ν the frequency. To calculate α from the absorbance we use the relation[16]

$$\alpha = \frac{(2.3 \times 10^3) A \delta}{M_w c l} \tag{2}$$

where A is the absorbance, δ, M_w, and c are the density, molecular weight and concentration of selenium respectively, and l is the path length of the cell.

Figure 3 shows this linear variation for the $w = 20$ sample at specific times. For all values of w, a shift in the band gap to lower energies was observed as the particle grew, but this particular sample showed the largest shift in band gap over the observed time period due to the slower reaction rate at larger w. The variation of band gap with particle size is consistent

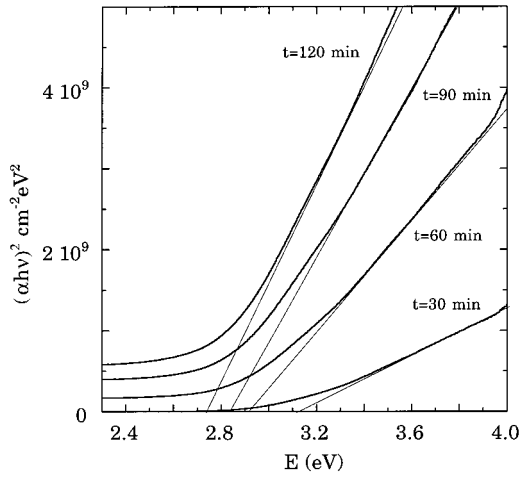

Figure 3. Variation of $(\alpha h\nu)^2$ vs $h\nu$ for $w = 20$. Band gaps are obtained from the intercepts of straight lines.

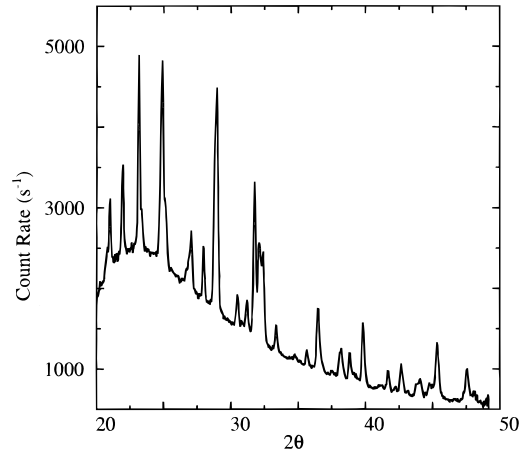

Figure 4. X-ray diffraction pattern for α-monoclinic selenium particles.

with the formulation given by Brus:[17]

$$\Delta E_g = \frac{h^2\pi^2}{2R^2}\left(\frac{1}{\mu}\right) - \frac{1.8e^2}{\epsilon R} \quad (3)$$

where ΔE_g is the change in the band gap due to quantum confinement, R is the particle radius, and $1/\mu = (1/m_e + 1/m_h)$ is the combined effective mass of the electron and hole. In the case of selenium, the second term is about 1% of the first and so can be ignored to a first approximation; the increase in band gap is then inversely proportional to the square of the particle radius. There is a wide spread of literature values for the effective mass of the electron and hole in amorphous and trigonal selenium,[18−20] but it is generally understood that the hole has a large effective mass compared with the electron and can be omitted in the expression for μ. For a-Se, which has a similar band gap to m-Se, the electron has an effective mass of approximately $0.25m_0$, where m_0 is the free electron mass. Using this value in eq 3, we can calculate approximate particle sizes from observed shifts in the band gap. For example, a value $\Delta E_g = 0.6$ eV gives a particle of 160 Å diameter after a reaction time of 15 min, which is in good agreement with TEM results.

X-ray diffraction spectra taken of the precipitate (Figure 4) showed that, at this stage, the sample was predominantly crystalline (α-monoclinic). Estimates of particle size can be obtained from the peak widths, $\Delta(2\theta) = 0.94\lambda/L \cos\theta$, where $\Delta(2\theta)$ is the full width half-maximum measured in radians, λ is wavelength, and L is the particle diameter.[21] Sizes of between

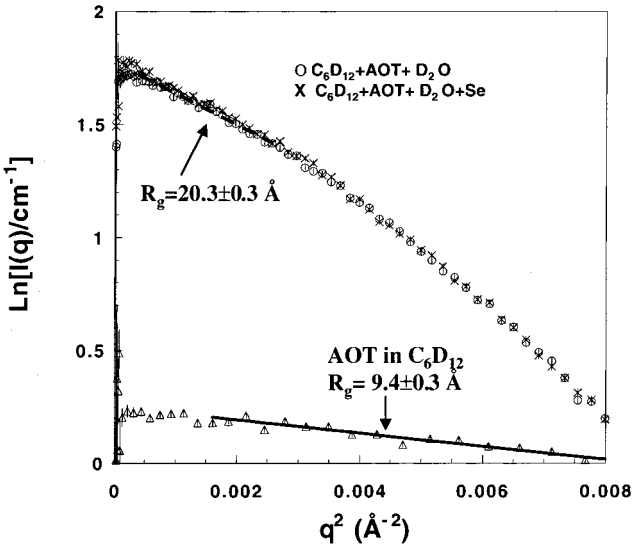

Figure 5. Guinier fits of micelles with and without selenium ($w = 10$) and for AOT in cyclohexane ($w = 0$).

350 and 500 Å were estimated after a reaction time of 2 h, when the particles had precipitated. Samples made at lower concentrations (less than 1.0×10^{-3} M) contained no other form of selenium; however, the faster reaction rate due to the increased concentration is believed to be the cause of the presence of a small amount of trigonal selenium apparent in the TEM pictures and X-ray diffraction patterns. Electron diffraction patterns of samples removed from the reverse-micelle solution in the first few minutes of reaction time showed amorphous material. We can therefore assume that a-Se forms initially but then transforms to m-Se.

SANS has been used to determine the size and shape of the micelles of AOT in C_6D_{12} and in the microemulsion AOT/D_2O/C_6D_{12} and to detect any changes due to the addition of selenium. For particles of volume V_p at number density n_p dispersed in a medium of scattering length density ρ_m, the differential scattering cross section $I(q)$ (cm^{-1}) may be written as

$$I(q) = n_p(\rho_p - \rho_m)^2 V_p^2 [S(q)\langle|F(q)|\rangle^2 + |\langle F(q)\rangle^2| - \langle|F(q)|\rangle^2] \quad (4)$$

where $P(q)$ $(=\langle|F(q)|^2\rangle$ is the single particle form factor arising from the size and shape of the particle.[22] $S(q)$ is the structure factor describing spatial correlations between particles and oscillates around 1 in the dilute region.

The differential neutron scattering cross section $I(q)$ was analyzed in the region $qR_g \leq 1.0$ by standard Guinier analysis[23]

$$I(Q) = I(0)\exp(-q^2R_g^2/3) \quad (5)$$

where the radius of gyration R_g is the root-mean-square distance of the neutron scattering density from the centroid. From a plot of $\ln[I(q)]$ vs q^2, a linear fit can be made in the region where $qR_g = 1.0$, and R_g can be calculated from and the scattering intensity at $q = 0$, $I(0)$, from the y intercept. Figure 5 shows the Guinier plots for the AOT microemulsion and the AOT/D_2O microemulsion in C_6D_{12}. The measured R_g value for the AOT micelles is 9.4 ± 0.3 Å and the $I(0)$ value is 1.325 ± 0.13 cm^{-1}. This corresponds to a spherical radius of 12.1 ± 0.4 Å, which agrees quite well with the results in the literature.[24] The molecular weight and hence the aggregation number can

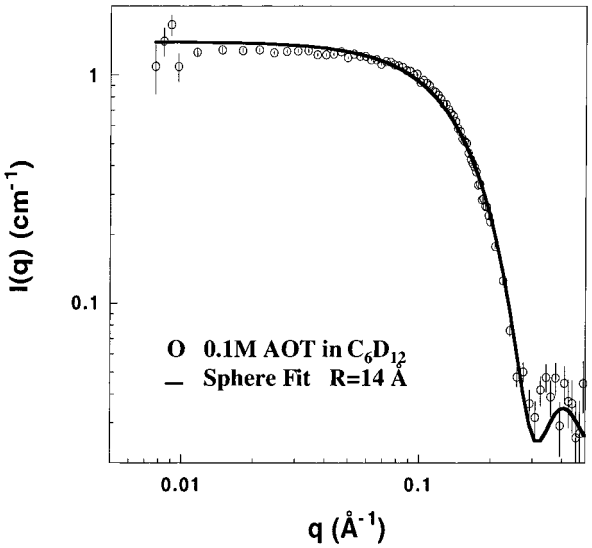

Figure 6. SANS data of AOT in cyclohexane fitted to a spherical model.

be derived from $I(0)$ by:

$$M_W = \frac{1000I(0)d^2N_A}{c(\rho_p - \rho_s)^2} \quad (6)$$

where N_A is Avogadro's number, c and d are the concentration and density of AOT, respectively, and ρ_p and ρ_s are the scattering length densities of AOT and C_6D_{12}, respectively. Using d = 1.1 g cm^{-3}, c = 44.5 mg/mL, $\rho_p = 0.62 \times 10^{10}$ cm^{-2}, and $\rho_s = 6.678 \times 10^{10}$ cm^{-2}, the molecular weight of the AOT micelles was found to be 5900 ± 580. This corresponds to an aggregation number of 13 ± 1, which agrees with the size of AOT micelles in C_6D_{12}.[25] Similar analysis gave R_g = 20.3 ± 0.3 Å for the micelles containing D_2O as well as D_2O + Se. Thus, the reaction forming Se nanoparticles does not alter the size of the micelles (see Figure 5).

The shape of the particles can be obtained by fitting the scattering data in the whole q region using the analytical functions available for different geometrical shapes. SANS data for the AOT micelles were fitted using the form factor for a sphere,

$$I(q) = I(0)\left(\frac{3\sin(qR) - qR\cos(qR)}{q^3R^3}\right)^2 + B \quad (7)$$

where R is the radius of the micelles and B is the incoherent background.

Figure 6 shows the data and fit for the micelles (w = 0) giving a radius of ~14 Å. This value is slightly larger than that of 12.1 ± 0.4 Å obtained from the Guinier analysis. It can be seen that the fit is reasonably good in the q region above 0.05 Å^{-1} but poor in the low q region, where the Guinier analysis was carried out. The latter may be due to a combination of interparticle effects due to the significant concentration of AOT (44.5 mg/mL) and some polydispersity in the sizes of the micelles.[26]

The scattering data for the reverse micelles containing D_2O and D_2O + Se have a secondary peak at q = 0.14 Å^{-1}, resembling a scattering function from a spherical shell. Our attempts to represent the data by using scattering functions for either ellipsoidal or cylindrical models led to poor fits. In the absence of information on the interaction potentials between the reverse micelles in organic solvents, we used the spherical shell model where $I(q)$ is given by the following equation:

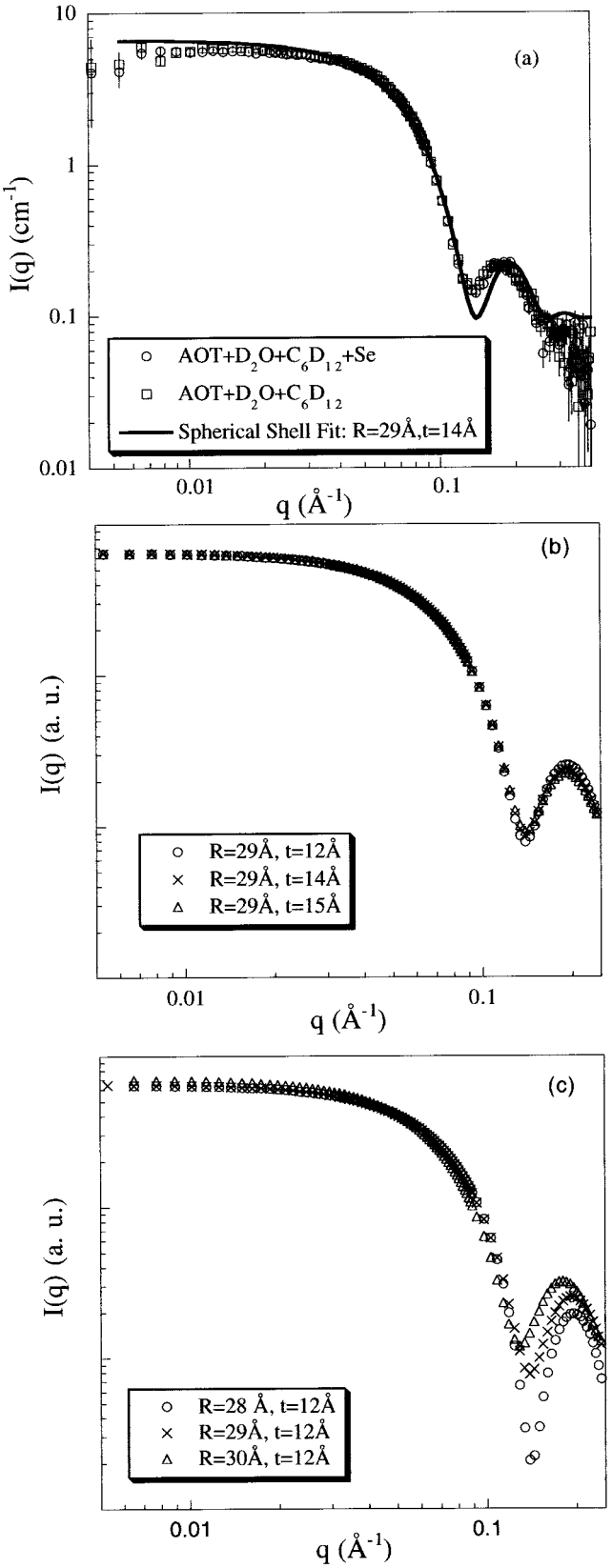

Figure 7. (a) SANS data of AOT + D_2O and AOT + D_2O + Se in deuterated cyclohexane fitted to a spherical shell model. (b) Simulated data: the effect of variation in the outer radius, but constant shell thickness. (c) Simulated data: the effect of variation in the shell thickness, but constant radius.

$$I(q) = A\left\{\frac{4\pi R^3}{3}(\rho_m - \rho_s)\left(\frac{3\sin(qR) - qR\cos(qR)}{q^3R^3}\right) + \frac{4\pi R_1^{\,3}}{3}(\rho_s - \rho_c)\left(\frac{3\sin(qR_1) - qR_1\cos(qR_1)}{q^3R_1^{\,3}}\right)\right\}^2 + B \quad (8)$$

In eq 8, A is a scale factor proportional to the concentration of the micelles, B is the incoherent background, R and R_1 are the radii of the whole particle and the core, respectively, and ρ_m, ρ_s, and ρ_c are the scattering length density values of C_6D_{12}, AOT, and D_2O, respectively. Figure 7a shows the results for a microemulsion with a radius of $\sim 29 \pm 1$ Å and a shell thickness of the micelles of $\sim 14 \pm 1$ Å. Overall, there is a good agreement between the model and the data; the small misfit may result from the polydispersity in the sizes of the micelles. Our simulations (parts b and c of Figure 7) showed that the peak will shift to lower q if the particles are larger, while the peak height will increase with decreasing thickness of the AOT shell. Other authors[26] have found evidence for cylindrical micelles in the presence of other surfactants such as lethicin and cetylpyridinium salicylate (CPS), but this is not the case here. Eastoe et al[27] found a spherical to cylindrical structural transformation of the micelles and back again on the addition of increasing amounts of water; however, the micelles became spherical with the formation of PbS nanoclusters.[14] Hirai et al[24] suggest the presence of a small amount of reverse micellar oligomers and give a length of 12 Å for an AOT molecule, confirming that the shell consists of one layer of AOT molecules.

The data and fit for selenium in the micelles are shown in Figure 7a; there is no reduction in the micelle size with the addition of selenium and no change in shape or thickness. Eastoe[14] found that the size of the micelles was unaffected by the conditions of the reaction when forming PbS and Hirai et al.[28] reported the same result in the presence of α-chymotripsin.

4. Conclusions

The synthesis of small particles of selenium in reverse micelles has been successfully carried out with a relatively simple procedure that may be preferred to existing preparation methods. The nanoparticles are formed within the first 5 min of reaction time and can be filtered from the solution. The crystalline particles were found to be spherical with an α-monoclinic structure and a size distribution on a nanometer scale. An increase in the band gap was observed by optical spectroscopy. The SANS results yield the size and shape of the micelles and reveal that selenium produced no change in either the size or structure. Future work will examine the micelles in the presence of other materials, particularly those not formed by ionic precipitation as in the present case.

Acknowledgment. We are grateful to D. Wozniak and the Operations Staff of the Intense Pulsed Neutron Source for experimental assistance and to A. Alatas, A. Goldbach, H. P. Hauck, S. Mini, and Y. Takayama for helpful discussions. This work was supported by the Divisions of Materials Sciences and Chemical Sciences, Office of Basic Energy Sciences, U.S. Department of Energy, under Contract W-31-109-ENG-38.

References and Notes

(1) Pileni, M. P. *J. Phys. Chem.* **1993**, *97*, 6961.
(2) Ungar, P.; Cherin, P. *The physics of Selenium and Tellurium*; Cooper, W. C., Ed.; Pergamon: Oxford 1969; p 223.
(3) Cherin, P.; Ungar, P. *Acta Crystallogr*. **1972**, *B28*, 313.
(4) Foss, O.; Janickis, V. *J. Chem. Soc., Dalton Trans.* **1980**, 624.
(5) Zhu, Y.; Qian, Y.; Huang, H.; Zhang, M. *Mater. Lett.* **1996**, *18*, 119.
(6) Zhang, H. Y.; Hu, Z. Q.; Lu, K. *Nanostruct. Mater.* **1994**, *5* (1), 41.
(7) Armand, P.; Saboungi, M. L.; Price, D. L.; Iton, L.; Cramer, C.; Grimsditch, M. *Phys. Rev. Lett.* **1997**, *79* (11), 2061.
(8) Goldbach, A.; Iton, L.; Grimsditch, M.; Saboungi, M. L. *J. Am. Chem. Soc.* **1996**, *118*, (8), 2004.
(9) Dimitrijevic, N. M.; Kamat, P. V. *Langmuir* **1988**, *4*, 782.
(10) Crawford, R. K.; Thiyagarajan, P.; Epperson, J. E.; Trouw, F.; Kleb, R.; Wozniak, D.; Leach, D. *PSI-Proc.* **1996**, *95*−*102*, 99.
(11) Thiyagarajan, P.; Epperson, J. E.; Crawford, R. K.; Carpenter, J. M.; Klippert, T. E.; Wozniak, D. *J. Appl. Crystallogr.* **1997**, *30*, 280.
(12) Eastoe, J.; Young, W. K.; Robinson, B. H.; Steytler, D. C. *J. Chem. Soc., Faraday Trans.* **1990**, *89*, 2883.
(13) Cowley, J. M. *Diffraction Physics*; North-Holland Publishing Company; Chapter 5.
(14) Eastoe, J.; Cox, A. *Colloids Surf. A* **1995**, *101*, 63.
(15) Knights, J. C.; Davis, E. A. *Solid State Commun.* **1972**, *11*, (4).
(16) Mills, G.; Zongguan, L.; Meisel, D. *J. Phys. Chem.* **1988**, *92* (3).
(17) Brus, L. *J. Phys. Chem.* **1986**, *90*, 2555.
(18) Beyer, W.; Mell, H.; Stuke, J.*Phys. Status Solidi B* **1971**, *45*, 153.
(19) Tutihasi, S.; Chen, I. *Phys. Rev.* **1967**, *158* (3), 623.
(20) Siemsen, K. J.; Fenton, E. W. *Phys. Rev.* **1967**, *161* (3), 632.
(21) Warren, B. E. *X-ray diffraction*; Addison-Wesley: New York, 1969; Chapter 13.
(22) Kotlarchyk, M.; Chen, S. H.; Huang, J. S. Kim, M. W. *Phys. Rev. A* **1984**, *29*, 2054.
(23) Guinier, A.; Fournet, G. *Small Angle Scattering of X-rays*; John Wiley and Sons: New York, 1955.
(24) Hirai, M.; Kawai-Hirai, R.; Yabuki, S.; Takizawa, T.; Hirai, T.; Kobayashi, K.; Amemiya, Y.; Oya, M. *J. Phys. Chem.* **1995**, *99*, 6652.
(25) Gorski, N., Ostanevich, Y. *Ber. Bunsen-Ges. Phys. Chem.* **1990**, *94*, 737.
(26) Schurtenberger, P.; Jerke, G.; Cavaco, C.; Pedersen, J. S. *Langmuir* **1996**, *12*, 2433.
(27) Eastoe, J.; Steytler, D. C.; Robinson, B. H.; Heenan, R. K.; North, N. A.; Dore C. J. *J. Chem. Soc., Faraday Trans.* **1994**, *90*, 85.
(28) Hirai, M.; Takizawa, T.; Yabuki, S.; Kawai-Hirai, R.; Hirai, T.; Oya, M.; Nakamura, K.; Kobashi, K.; Amemiya, Y. *J. Chem. Soc., Faraday Trans.* **1995**, *91*, (7) 1081.